



Full length article

Astro Space Locator — A software package for VLBI data processing and reduction

S.F. Likhachev, I.A. Girin, V. Yu. Avdeev, A.S. Andrianov, M.N. Andrianov, V.I. Kostenko, V.A. Ladygin, A.O. Lyakhovets, I.D. Litovchenko, A.G. Rudnitskiy*, M.A. Shchurov, N.D. Utkin, V.A. Zuga

Astro Space Center, Lebedev Physical Institute, Russian Academy of Sciences, Profsoyuznaya str. 84/32, Moscow, 117997, Russia

ARTICLE INFO

Article history:

Received 21 February 2020

Accepted 17 September 2020

Available online 23 September 2020

MSC:

85-04

Keywords:

Methods: data analysis

Techniques: image processing

Techniques: interferometric

ABSTRACT

The article describes the main features and algorithms of Astro Space Locator (ASL) software package. This high performance package has a user-friendly graphical interface and it is used for VLBI data processing and reduction. ASL supports data editing, calibration, multi-frequency analysis, standard and multi-frequency VLBI imaging.

© 2020 Elsevier B.V. All rights reserved.

1. Introduction

Radio interferometry is a well-developed technology that allows obtaining information about the Universe in the radio-frequency range.

Therefore, it is necessary to develop high-performance VLBI data processing systems. One of the most important components of VLBI data processing is the reconstruction of images from VLBI data, which provides astronomers with direct visual information about structure of objects under study, thus making possible to determine their characteristics.

Effective software is essential for reliable scientific results in VLBI. Since the work with experimental data requires the use of appropriate mathematical software, its development, maintenance and support are critical for any astronomical project (Thompson et al., 2017).

Currently, there are many reliable software packages that perform calibrations, data editing, VLBI imaging and analysis (for example, Difmap, AIPS, CASA, PIMA, VNSIM etc.) (Shepherd, 1997; Palmer, 1996; Jaeger, 2008; Petrov et al., 2011; Zhao et al., 2019).

Most of them lack a convenient graphical interface. Some of the programs could have a relatively narrow scope of application for VLBI data processing, like Difmap has the only function to reconstruct VLBI images.

In this paper we describe the Astro Space Locator software package, the purpose of which is to combine all the tools for editing, calibration, post-correlation processing and analysis of VLBI data. It consists of a set of basic routines and additional tools 2. Section 3 describes the VLBI data visualizer (VisView); Section 4 is devoted to the VLBI data editing program (Editor); Section 5 deals with a procedure for calibrating radio interferometric data; Section 6 presents the details of fringe fitting; Section 7 describes an image recovery reconstruction program (Imager); Sections 11 and 12 are about tools and algorithms implemented in the ASL for processing of specific source types (pulsars in Section 11 and masers in Section 12); Section 13 discusses a Modeler program for simulation of observations; Section 14 describes Utilities; and Section 15 presents the conclusions.

2. Overview

The software package was developed using object-oriented programming technology (Rumbaugh, 1991; Booch, 1993) for Microsoft Windows in C++ language using Microsoft Foundation Classes (MFC). It is possible to run ASL on some Linux distributive (Ubuntu and Fedora) and MacOS using Windows emulation software (WINE, Parallels, etc.). All tools and application interfaces in the package are standardized and have modular design. Such

* Corresponding author.

E-mail addresses: slikhach@asc.rssi.ru (S.F. Likhachev), igirin@asc.rssi.ru (I.A. Girin), adisonmail@gmail.com (V.Y. Avdeev), andrian@asc.rssi.ru (A.S. Andrianov), mihail-andrian@asc.rssi.ru (M.N. Andrianov), vkostenko@asc.rssi.ru (V.I. Kostenko), ladygin@asc.rssi.ru (V.A. Ladygin), lyakhovets@asc.rssi.ru (A.O. Lyakhovets), grosh@asc.rssi.ru (I.D. Litovchenko), arud@asc.rssi.ru (A.G. Rudnitskiy), shaddowman@mail.ru (M.A. Shchurov), nikitautkin@asc.rssi.ru (N.D. Utkin), zuga@asc.rssi.ru (V.A. Zuga).

Table 1
Comparison of the functionality of various VLBI data processing software packages.

	ASL	AIPS	CASA
GUI	+	-	+/-
Various convolution kernel functions	+	-	+
Robust weighting	-	+	+
Image cubes	-	+	+
Various kernel functions (tapering/gridding)	+	-	-
Multi-threading	+	-	+
VLBI simulations	+	-	+
Easy installation	+	-	+

an approach allows easy replacement or addition of new methods and features, making ASL an adaptable software. Moreover, the package interface was developed based on the “What You See Is What You Get” (WYSIWYG) approach in order to make the user-data interaction as simple, direct and transparent as possible.

Special attention was paid to optimization of data processing and analysis algorithms in order to minimize the use of RAM memory and disk space. Most part of the well-known algorithms and computational procedures were re-written to increase the computational efficiency (for example, fringe-fitting, calibrations, CLEAN). Some of the algorithms, like self-calibration and multi-frequency synthesis were done from scratch.

Because post-correlation data processing is multi-stage and iterative, its automation is of great importance. Fortunately, the ASL allows convenient management of meta-information: it includes a wide range of methods for data editing and supports direct data flagging. A conceptual diagram of the Astro Space software package is shown in Fig. 1. In general, it keeps with the logic and sequence of VLBI data processing stages: data visualization, editing, calibration and fringe fitting, self-calibration and imaging.

Noteworthy is that the ASL supports all main VLBI data formats, such as IDIFITS,¹ UVF² and UVX. UVX file format is a VLBI data format of ASC Correlator (Likhachev et al., 2017). Therefore, the package is compatible with all known VLBI data processing software.

As it was mentioned, one advantage of ASL is convenient graphic interface. Software package does not require specific skills in working with command line. During operation ASL is able to save any data as table in text file. In addition there is possibility to select and edit data directly in the tables.

Another feature of ASL is convenient graphical representation of the data. Each data plot has a number of interactive tools, like: zoom in/out, cross-section, save data as image and save data as text.

Table 1 shows the comparison of key features between ASL and other VLBI data reduction software.

Detailed description of various kernel functions for tapering and gridding is presented in Section 8.1, description of VLBI simulations is presented in Section 13.

3. Data visualization

The VisView program visualizes correlated VLBI data. It has many options and allows various primary analyses of interferometer data in various ways. Since all correlated VLBI data are complex values, one can select and analyze any of their components [real part, imaginary part, amplitude (modulus), phase (argument)] both in 2D and 3D diagrams.

¹ The FITS Interferometry Data Interchange Convention: <ftp.aoc.nrao.edu/pub/software/aips/TEXT/PUBL/AIPSMEM114.PS>.

² AIPS FITS Format: <ftp.aoc.nrao.edu/pub/software/aips/TEXT/PUBL/AIPSMEM117.PS>.

3.1. Two-dimensional diagrams

For each combination of baseline, selected time interval and bandwidth, the following diagrams can be generated: visibility vs. delay, power spectrum vs. frequency, visibility vs. time and power spectrum vs. time.

For each observation time point the plot shows the maximum value of the visibility (or power spectrum) for all delays (or frequencies).

3.2. Three-dimensional diagrams

3D plots present visibility-time-delay and spectra-fringe rate-frequency relationships.

The program performs Fourier transform along the selected variables.

1. The Dynamic spectrum (Frequency–Time) diagram shows the spectrum behavior over time. See Fig. 2 (left).
2. The Fringe rate–Frequency diagram shows the distribution of spectra from fringe rate.
3. The Delay–Time diagram displays the behavior of correlation function over time and delay.
4. The Fringe rate–Delay diagram shows the behavior of correlation function over delay and interference frequency. See Fig. 2 (right).

The VisView can be used to obtain various cross-sections and projections of the described 3D diagrams. For example, taking a cross-section of dynamic auto-spectrum along the frequency axis yields a spectrum for a selected time. It is also possible to approximate the resulting cross-section with polynomials or to make an average projection on any two of the three dimensions of the diagram.

4. Data editing

The ASL package includes an editing program, the Editor, for VLBI data editing and correction. The correlated VLBI data (including any components of complex visibility function and spectrum) can be edited both manually and automatically (Girin et al., 2006). The Editor also supports approximation, smoothing and other mathematical manipulations on the data. The Editor consists of two parts: operations with data files and data editing.

4.1. Data file operations

This part includes data format converting: IDIFITS and UVF formats can be converted to UVX and vice versa. Thus, the user can get the corrected IDIFITS, UVF or UVX and make the next stage of its processing with any other software if necessary.

The Editor includes data averaging in frequency and in time. Correspondingly, there are two types of averaging: vector (real and imaginary parts are averaged separately) and scalar [module (amplitude) and argument (phase) are averaged separately].

It is possible to average the value of spectral intensity either over the whole IF bands or over groups of individual channels. In the last case the user can choose number of channels in group. Average signal can be attributed to either central or the first frequency of the selected frequency range.

4.2. Editing

The following data editing options are available in the Editor: telescopes and baselines editing, time editing, spatial editing of (u, v, w) information, frequency editing. It is possible to choose editing:

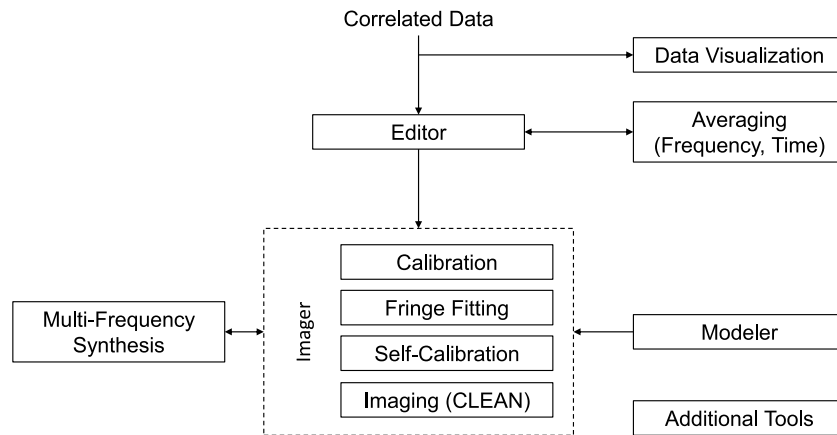


Fig. 1. Conceptual diagram of Astro Space Locator software package.

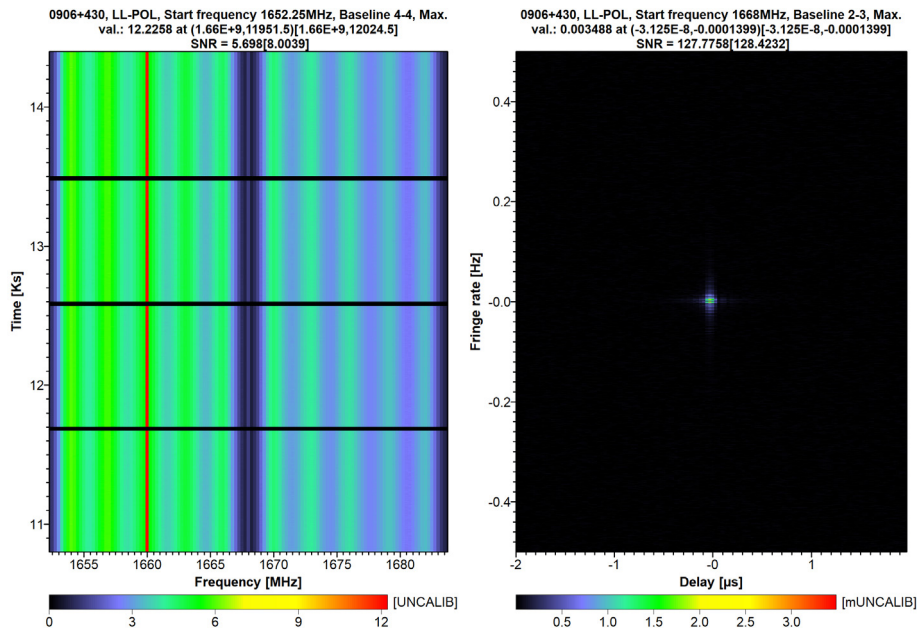


Fig. 2. Example of three-dimensional diagrams obtained in VisView: dynamic spectra (“Frequency–Time” diagram, left) and “Delay–Fringe rate” diagram (right).

1. Component of visibility function. Select which component to be displayed and edited;
2. Weight of individual observation that takes into account contribution of errors;
3. Polarization state. In case the UVX file contains information about several polarizations, it is possible to remove any of them;
4. Frequency IDs – any frequency ID can be kept or removed;
5. Frequency Band – any frequency band can be kept or removed.

4.3. Telescopes and baselines editing

In telescope and baseline editing it is possible to select which data to remove or keep in UVX file. Interface displays the (u, v) coverage with the modified data.

4.4. Time editing

Components of visibility function (amplitude, phase, real part, imaginary part) can be displayed either in tables or in plots for the selected time interval. The values of visibility function

components can be edited directly. For plot editing more options are available:

1. Approximation of “Time-Visibility function component” plot.

Several ways of approximation function are provided:

- Chebyshev polynomials;
- Fourier series expansion;
- Simple polynomial approximation;
- Auto mode – choice between three variants mentioned above that corresponds to minimal variance between data and fitting.

Fig. 3 shows an example of amplitude and phase editing data plots.

2. Selection of plot region. In general, several operations with points in the selected region can be done. Both points corresponding to single baseline and points that correspond to all baselines in the selected plot region can be edited.

- Data flagging/unflagging. Flagged points will be ignored in further analysis and processing;

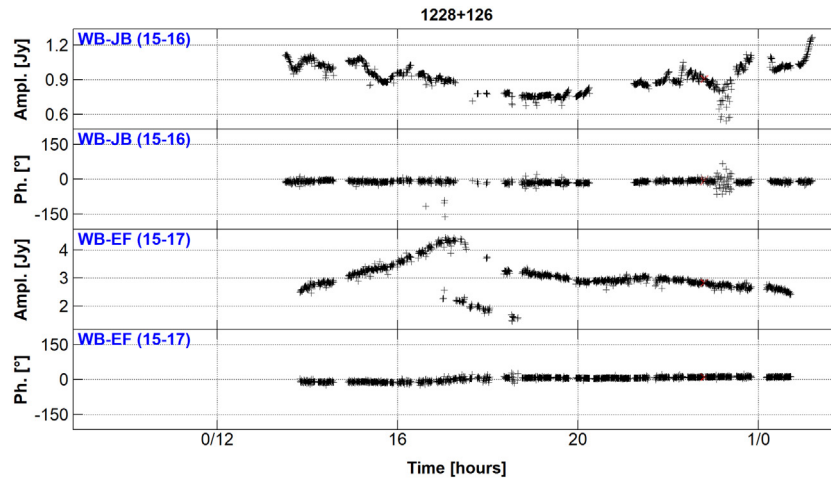


Fig. 3. Example of plot showing editing of visibility amplitude and phase in time. From top to bottom: baseline WB-JB amplitude and phase, baseline WB-EF amplitude and phase. Data sample of Radioastron mission imaging observations of M87 (1228+126) at L-band (18 cm or 1668 MHz), date/time of observation: 04.06.2014 09:00:00–05.06.2014 01:30:00. Data points can be selected interactively on plot and flagged/unflagged.

- Editing the values of visibility function components in table, one can choose any of them to conduct approximation;
- Offset the values;
- Statistical analysis.

The program can calculate the histogram over values of visibility function component. In addition Gaussian distribution test can be made. Along with histogram, mean value, dispersion and a message whether displayed distribution corresponds to Gaussian are provided.

4.5. Spatial editing

Here visibility component is displayed as function of coordinates and distances in Fourier-space. One can choose as independent variable:

- Individual (u), (v) or (w)-coordinate.
- Distances in (u, v, w) space: $R(u, v) = \sqrt{u^2 + v^2}$, $R(v, w) = \sqrt{v^2 + w^2}$, $R(u, w) = \sqrt{u^2 + w^2}$, $R(u, v, w) = \sqrt{u^2 + v^2 + w^2}$.
- (u) and (v)-coordinates – here (u, v) coverage is displayed with values of visibility function components.

Fig. 4 shows an example of spatial editing for the case of visibility vs. $R(u, v)$. Along with operations mentioned above, one can make the following actions:

- Beam synthesis using chosen observational points on plot, beam is approximated as ellipse.
- Approximation of data by Gaussian function and possibility of flagging/unflagging points with a given threshold of $n\sigma$ ($n = 1, 2, \dots, N$).
- Calculation of integral of Gaussian approximation function within the chosen region of the data.

4.6. Frequency editing

Frequency editing is capable of editing the values in individual frequency channels of the correlated spectrum and differential phase calculation. The last one is a subtraction of visibility phase in one chosen channel from visibility phases of other channels.

5. Calibration

Many factors contribute to recorded signal from observed sources, thus any VLBI data must be calibrated. The calibration procedure consists of the following steps: correction of quantization errors using auto correlation functions, correction for different levels of signal quantization on telescopes, amplitude calibration, bandpass correction.

All calibration tasks are gathered in Calibration subroutine. First three steps are performed as a part of amplitude calibration function.

5.1. Amplitude calibration

1. Correction of digital errors accounts for quantization errors of the original signals using auto correlation functions $r(i, k, m, t)$. Cross-spectra calibration assumes that parameters of the digital signal converter are known. In practice, these parameters may not be optimal or are not known with sufficient accuracy. This leads to the errors in measurement of cross-correlation spectra amplitude. These errors can be estimated by measuring the average value of the auto correlation spectrum of the antennas (Kogan, 1995).

$$S_{calib}(i, j, k, l, mm, t) = \frac{S_{uncalib}(i, j, k, l, mm, t)}{\sqrt{r(i, k, m, t)r(j, k, m, t)}}, \quad (1)$$

where i, j – telescope indices, k – number of frequency band (IF), l – frequency channel, m – polarization, t – time, mm – Stokes parameter, $r(i, k, m, t)$ – average value of auto-spectrum amplitude for i^{th} antenna in chosen frequency band, $S(i, j, k, l, mm, t)$ – spectrum.

2. Van Vleck correction is a correction of different quantization levels of the received signal. For example, 1-bit quantization was used in Radioastron, while ground telescopes used 2-bit quantization in joint ground-space VLBI observations.

Conversion of digital spectra S_d into corrected spectra S_a is determined by the following relation:

$$S_a(i, j, k, l, mm, t) = \frac{S_d(i, j, k, l, mm, t)}{\sqrt{B_i(N_q)B_j(N_q)}}, \quad i \neq j \quad (2)$$

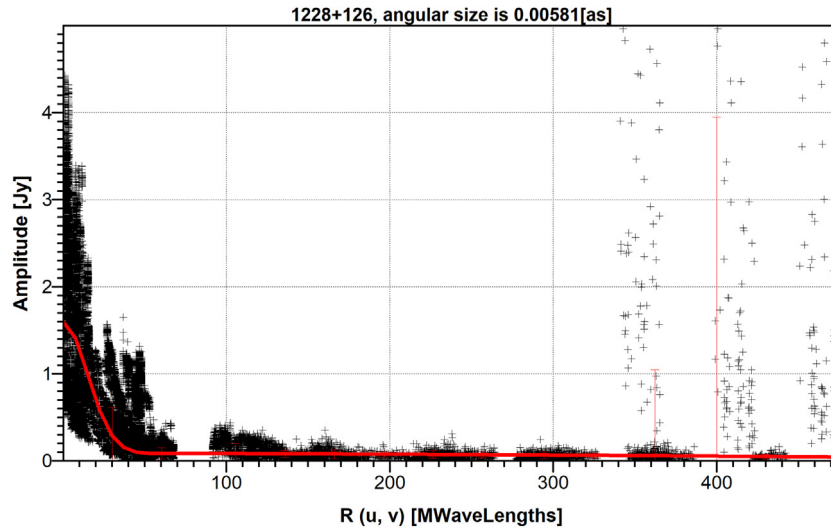


Fig. 4. Example of spatial editing of visibility function on the “Visibility vs. Baseline projection” plot. Data sample of Radioastron mission imaging observations of M87 (1228+126) at L-band (18 cm or 1668 MHz), date/time of observation 04.06.2014 09:00:00–05.06.2014 01:30:00. Visibility data are shown as black crosses. Red line shows a Gaussian approximation of the unflagged data. Any data can be selected interactively on plot, flagged/unflagged or modified in amplitude value.

3. Correlation flux. This procedure recalculates correlated amplitude of signals r into correlated flux F in Jy . The procedure requires an ANTAB³ file containing information about noise temperature of telescopes receiving system, as well as information (polynomial parameters) about sensitivity/elevation dependence.

$$F(i, j, k, l, mm, t) = \frac{r(i, j, k, l, mm, t)}{\sqrt{SEFD(i, k, m, t) \cdot SEFD(j, k, m, t)}}, \quad (3)$$

where $SEFD(i, k, m, t)$ – system equivalent flux density in Jy .

5.2. Bandpass

Bandpass procedure corrects the shape of the receiver bandwidth. Signal amplitude, phase or both can be calibrated.

- Amplitude bandpass corrects the shape of the receiver bandwidth using averaged auto-spectrum from calibration source:

$$F_{calib}(i, j, k, l, mm, t) = \frac{F_{uncalib}(i, j, k, l, mm, t)}{\sqrt{A(i, k, l, m, t)A(j, k, l, m, t)}} \quad (4)$$

where $A(i, k, l, m, t)$ and $A(j, k, l, m, t)$ are average auto-spectrum of calibration source.

- Phase bandpass calibration uses the phase of calibration source cross-spectra that is approximated linearly. The parameters of this linear approximation then are used to adjust the phase of observed source. Corrections are applied for each spectral channel.

5.3. External gain file calibration

There is also a possibility to apply calibration from an external gain file. For example, this can be an external file with gain coefficients obtained from self-calibration, calibration source fringe fitting or phase transferring procedures (Sections 6 and 9).

³ Generating ANTAB T_{sys} files: <https://ivsc.gsfc.nasa.gov/meetings/tow2011/Campbell.MW.pdf>.

6. Fringe fitting

The visibility function obtained after correlation may contain errors related to inaccurate clocks at VLBI stations, inaccurate frequency setup or various delays related, for example, to the troposphere. In the case of space telescope, additional errors arise from the accuracy of the orbit determination. To eliminate such errors there is a utility in ASL that performs fringe fitting. Astro Space Locator has two modes of fringe fitting: baseline-based and global.

Implementation of baseline-based fringe fitting is the following:

1. Selection of value of time interval of solution search T_{int} . The value of T_{int} can be estimated based on the atmosphere coherence time.
2. Calculation of matrix C for each baseline on each T_{int} time interval. The elements of this matrix ($C_{i,j} = A_{i,j}e^{i\phi_{i,j}}$): $A_{i,j}$ and $\phi_{i,j}$ are amplitude and phase of cross-spectrum at i th spectral channel for j th moment of time respectively.
3. Fourier transform of matrix C from “time-frequency” to “delay-fringe rate” domain and search for maximum of obtained matrix. At the first step fringe fitting subroutine in ASL search for rectangle area with a total visibility amplitude maximum in “delay-fringe rate” matrix. At the second step the subroutine looks for the maximum value inside this selected rectangle. Detected fringe must satisfy to the following condition: residual delay and fringe rate of the peak must have close values in different time intervals T_{int} . At the peak phase of visibility function ϕ_0 , shift of delay τ and shift of fringe rate f_{fr} are determined.
4. Calculation of phase correction terms (gains) for each baseline:

$$\phi_k = \phi_{0k} + 2\pi(t - t_0)f_{fr} + 2\pi(f - f_0)\tau_k \quad (5)$$

Here k is a telescope index.

5. Applying of gain coefficients to baseline:

$$\phi_{ij}^{new} = \phi_{ij} + \phi_k \quad (6)$$

Global fringe fitting algorithm differs from baseline-based fringe fitting by the following points:

1. Selection of reference station. Reference station can be selected both manually and automatically. In the latter case reference telescope will be one that has the largest number of baseline with other telescopes.
2. Estimation of ϕ_0 , τ and f_{fr} for each telescope that has a baseline with reference antenna. Values of ϕ_0 , τ , f_{fr} for reference antenna are taken to be equal to zero.
3. Formation and solution of system of phase closure relations for ϕ_0 for all possible triplets of telescopes.

$$\phi_c = \phi_{12} + \phi_{23} + \phi_{31} + \text{noise} \quad (7)$$

Phase closure relations provide possibility to calculate gains even for baselines with low signal-to-noise correlation, making this algorithm applicable for observations of weak sources.

4. Applying of antenna gains to baselines is performed in the following way:

$$\phi_{ij}^{new} = \phi_{ij} + (\phi_a - \phi_b), \quad (8)$$

where a and b are telescope indices of ab baseline .

However, unlike baseline-based fringe fitting algorithm, global fringe fitting allows to find only relative errors rather than absolute. In addition, global fringe fitting algorithm requires either information about the source model or point (unresolved) calibration source. From the other hand, baseline-based fringe fitting is applicable only for baselines that have correlation and the algorithm does not work for faint sources with low signal-to-noise ratio correlation.

Implementation of fringe fitting in ASL package provides possibility to compensate not only linear phase drift, but also errors in quadratic term $\tau = a_2(t - t_0)^2$ of geometric delay model, which is particularly important for Space-VLBI, because the accuracy of quadratic term of the delay can be large in this case. Thus, the influence of space radio telescope acceleration uncertainties on the signal-to-noise ratio and signal coherence can be significant. Quadratic term compensation in the fringe fitting can improve the resulting correlated amplitude and coherence. Fig. 5 demonstrates correlated amplitude after fringe fitting done with ASL with (bottom panel) and without (middle panel) quadratic term compensation for one of the Radioastron experiments. As it can be seen, introducing the quadratic term in fringe fitting significantly improve the coherence and reduces the fluctuations of correlated amplitude.

Gains, obtained by fringe fitting procedure, can be used to improve the delay model for correlator, which is important for Space-VLBI. They can also be used in procedure for calibration of tropospheric and ionospheric phase fluctuations.

Atmospheric phase corrections are necessary to improve the efficiency of VLBI observations, especially at higher frequencies. One of methods that use the advantage of simultaneous multi-frequency observations is Frequency Phase Transform (FPT) (Rioja et al., 2011). This method is already used in data processing of Korean VLBI Network (KVN). KVN has a unique quasi optical system designed to separate the signal into different frequency bands. Such system provides capabilities to perform simultaneous observations at four frequencies (Kim et al., 2015).

Thus, the observations at two different frequencies simultaneously allow to perform phase transfer from lower frequency to higher one and to compensate delay in troposphere. Observations with three different frequencies allow to compensate the delay in ionosphere.

It is important to use such multi-frequency observations and perform phase transferring for the next generation millimeter VLBI missions, including Millimetron space-VLBI observatory. This can help to increase coherence time and sensitivity. The algorithms of FPT in Astro Space Locator are currently under testing.

7. Imaging

Imager is a component of the ASL package that solves the task of VLBI data image reconstruction. A complete mathematical solution of the image reconstruction problem in VLBI is non-trivial. One reason is the lack of knowledge of the original image (the “true” image of the radio source). Thus, one can only hope for procedures that provide some more or less reliable estimates of the original image obtained on the basis of the VLBI data analysis. The problem of image reconstruction is formalized, which allows us to present it as the following list of mathematical tasks: correlation analysis, phase and amplitude calibration, data approximation (weighing, gridding), image deconvolution.

This article will not address the issue of correlation analysis, since ASL is designed to work with correlated data. The details on the correlation procedure can be found in Likhachev et al. (2017). Calibration is described in Sections 5 and 6. This section of the article will concern the peculiarities of data approximation (7.1) and image deconvolution (8).

7.1. Data approximation

Estimation of the visibility function $V(u_i, v_i)$ at the points of the (u, v) plot is a stochastic problem due to the fact that observations are made by imperfect devices. In this case, different points of (u, v) coverage will have varying degrees of confidence. Typically, the degree of confidence in measurements is estimated by the weight $w \sim 1/\sigma^2(u_i, v_i)$ for the (u_i, v_i) data point. If the average value of the visibility function at the point (u_i, v_i) is \bar{V} then the probability density of getting the value $V(\mathbf{u})$, where \mathbf{u} is point with coordinates (u, v) , is equal to:

$$p(V(\mathbf{u})) = \frac{1}{\sqrt{2\pi}\sigma(\mathbf{u})} \cdot \exp\left(-\frac{[V(\mathbf{u}) - \bar{V}(\mathbf{u})]^2}{2\sigma^2(\mathbf{u})}\right) \quad (9)$$

Then the likelihood equation (for the value of the visibility function) can be represented as

$$\frac{dl}{d\bar{V}(\mathbf{u})} = \sum_u \frac{V(\mathbf{u}) - \bar{V}(\mathbf{u})}{\sigma^2(\mathbf{u})} \quad (10)$$

Its solution can be presented as follows:

$$\bar{V}(\mathbf{u}) = \frac{\sum_u w(\mathbf{u})V(\mathbf{u})}{\sum_u w(\mathbf{u})} \quad (11)$$

The resulting function $w(\mathbf{u})$ called weighing function indicates the degree of reliability of the measurement and assigns low weight to measurements with low accuracy. In Imager it is possible to select the type of weighing function – natural weight or uniform weight (Thompson et al., 2017).

The set of measured points can be represented as

$$V(\mathbf{u}) = \sum_{i=1}^N V^{[i]} \cdot \delta(\mathbf{u} - \mathbf{u}_i, v - v_i) \quad (12)$$

We denote $V^{[i]}$ as $V(\mathbf{u}_i)$ and consider the convolution procedure:

$$\begin{aligned} V_{approx}(\mathbf{u}) &= \varphi_\alpha(\mathbf{u}) \cdot \sum_{i=1}^N V(\mathbf{u}_i) \cdot \delta(\mathbf{u} - \mathbf{u}_i) = \\ &= \sum_{i=1}^N V(\mathbf{u}_i) \cdot \varphi_\alpha(\mathbf{u}) \cdot \delta(\mathbf{u} - \mathbf{u}_i) = \\ &= \sum_{i=1}^N V(\mathbf{u}_i) \cdot \varphi_\alpha(\mathbf{u} - \mathbf{u}_i) \end{aligned} \quad (13)$$

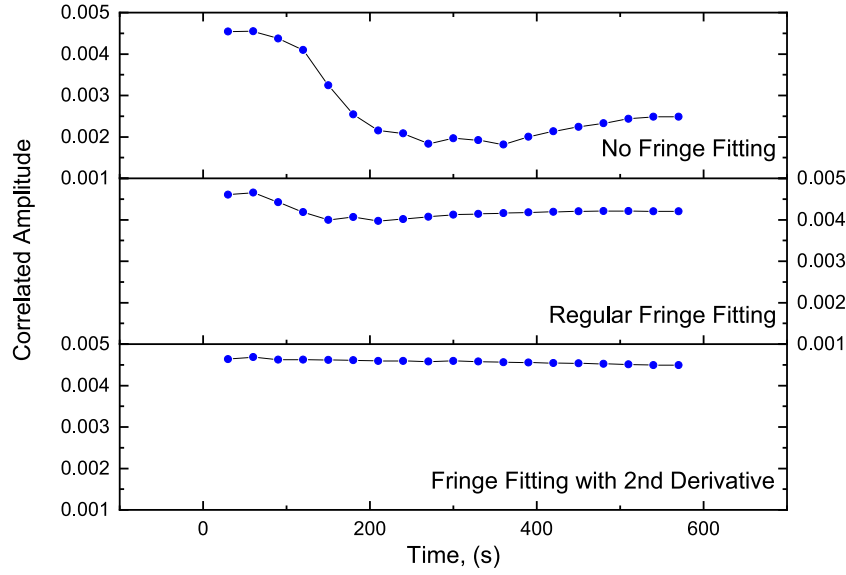


Fig. 5. Dependence of correlated amplitude from integration time before (top panel) and after regular fringe fitting (middle panel) and quadratic term compensation (bottom panel). Radioastron experiment, date/time: 11.12.2017 17:00–18:00, baseline Radioastron-Torun (RA-TR). Observation wavelength $\lambda = 6$ cm.

Thus (13) is a continuous approximation of the measured visibility function. The class of functions $\varphi_\alpha(x) = \frac{\psi_\alpha(x)}{\sum_\alpha \psi_\alpha(x)}$ is called the partition of unity.

Then the approximation by the continuous visibility function $V_{approx}(\mathbf{u})$ at the point \mathbf{u} can be represented as

$$V_{approx}(\mathbf{u}) = \frac{\sum_i \psi_i(\mathbf{u})V(\mathbf{u}_i)}{\sum_i \psi_i(\mathbf{u})} \quad (14)$$

Such procedure is called gridding convolution or gridding.

8. Image deconvolution

The procedure of image deconvolution can be divided into several stages:

1. Approximation of the discrete visibility function $V(u_i, v_i)$ by continuous one $V(u, v)$. Such approximation is possible only in the vicinity of $\alpha(u_i, v_i)$ of each point (u_i, v_i) .
2. Search for discrete values of $V(u_k, v_k)$ of the continuous function $V(u, v)$ at the studied points of the (u, v) -plane, i.e. at points of the calculated uniform grid. This procedure is called the re-sampling procedure (7.1).
3. Obtaining an estimate of the brightness distribution $I(x_k, y_k)$ in the form of the ratio between the Fourier transform (FFT) of $V(u_k, v_k)$ values and the FFT of the convolution kernel function (14).

8.1. Dirty map

Obtaining dirty map starts with the gridding procedure (7.1). (u, v) plane contains the information on the visibility functions V at each point of the (u, v) for the entire time of observation. The gridding procedure is applied to this plane. Thus, (u, v) plane is split into a number of cells. Visibility functions for the points inside each cell are approximated by $V_{approx}(\mathbf{u})$ (14).

In ASL Imager, the gridding procedure has several V_{approx} functions of the convolution kernel (14):

1. Averaging, i.e. $\psi = const$

$$V_{approx}(\mathbf{u}) = \frac{\sum_i V(\mathbf{u}_i)}{N}$$

where N is the number of points inside the cell;

2. Gaussian kernel

$$\psi(\mathbf{u}) = \exp \left[-\frac{1}{2} \left(\frac{u^2}{\sigma_u^2} + \frac{v^2}{\sigma_v^2} \right) \right]$$

where u, v are the coordinates of the (u, v) plane point, σ_u, σ_v is the grid cell width.

3. Lorentz kernel

$$\psi(\mathbf{u}) = \frac{8\pi^3 \alpha^3}{(4\pi^2 \alpha^2 + r^2)^{\frac{3}{2}}}$$

$$r = \sqrt{u^2 + v^2}$$

4. Hat-function

$$\psi(\mathbf{u}) = \frac{\sin(\sqrt{u^2 + v^2})}{\sqrt{u^2 + v^2}}$$

The capability to select different kernel function allows you to reduce image distortion images depending on an interferometer configurations or, in other words, depending on the (u, v) coverage (see, for example, Thompson et al., 2017, Section 10.2.4).

During the procedure of obtaining dirty map it is necessary to set the field of view (in angular seconds) and the number of cells along the axes ($2^n, n = 5 \dots 13$). Next follows the re-sampling procedure. Gridding is performed in such a way that the initial elements of this “grid” correspond to the elements of the (u, v) coverage closest to the origin, and the final ones are the elements farthest from it. Thus, if a 1024×1024 grid is superimposed on the (u, v) plane, then the output will be a square matrix of $V(\mathbf{u})$ with a size of 1024×1024 elements, in which the unfilled elements are zero, the rest are oversampled visibility functions of the corresponding (u, v) coverage region with the corresponding kernel, calculated with the corresponding weight.

The visibility function $V(u, v)$, defined on some (u, v) plane has an unlimited domain of definition. That is, there is no limited region beyond which this function is equal to zero. However, in real observations, this function is limited to a certain region determined by the characteristics of the interferometer. In this case, after truncating the infinite region of approximation of the visibility amplitude, distortions appear at the points of discontinuity of the function. This phenomenon is called the Gibbs phenomenon (Bates and McDonnell, 1986). To suppress this effect

Imager uses tapering function $T(u, v)$:

$$V_{taper}(u, v) = V(u, v) \cdot T(u, v) \quad (15)$$

The following tapering functions are available:

1. Uniform

$$T_\alpha(u, v) = 1;$$

2. Gaussian

$$T_\alpha(u, v) = \exp(-\alpha^2(u^2 + v^2));$$

3. Lorentz

$$T_\alpha(r) = \frac{2\pi\alpha}{(4\pi r^2 + \alpha^2)^{1.5}};$$

$$r = \sqrt{u^2 + v^2};$$

Tapering can improve the image by reducing artifacts that appear due to the contribution of interference at high spatial frequencies. During the image reconstruction procedure the visibility function will have non-zero values at the edges of the synthesized (u, v) plane. This is caused by multiplication of the visibility function values by a certain kernel function. Accordingly, in the general case, in order to correct this data distortion, it is necessary to use the tapering function that correspond to the following requirements: the function must be continuous, at the edges of the (u, v) plane it must take zero values, its integral must be equal to unity. Then, the tapering function eliminates the distortions introduced by the convolution kernel function at high spatial frequencies.

Tapering function is selected so that to achieve the best “signal-to-noise” ratio. Most commonly used is the Gaussian. However, there are cases, for example, when the (u, v) coverage is more or less uniform (for example, (u, v) coverage of VLA). In this case, it is recommended to use the uniform tapering function. Note, that in case ASL uniform tapering just turning off the tapering procedure. In general, the ability to use various tapering function in different situations is an advantage of the ASL package.

Returning to the imaging procedure, next, it is necessary to take the derivative matrix $B(\mathbf{u})$ obtained from $V_{approx}(\mathbf{u})$:

$$B(\mathbf{u}) = \begin{cases} 0, & \text{if } V_{approx}(\mathbf{u}) = 0 \\ 1, & \text{if } V_{approx}(\mathbf{u}) \neq 0 \end{cases}, \quad (16)$$

The two-dimensional Fourier transform of B will be the matrix $\tilde{B}(u, v)$, $\tilde{B}_{u,v} \in C$. Amplitudes of this matrix $\tilde{B}(u, v)$ describe the directional pattern of the interferometer or beam. Strictly speaking, it has the dependency $\sin(x)/x$, but can be well approximated by the following functions:

1. Two-dimensional Gauss function

$$g = A \cdot \exp \left[-\frac{1}{2} \left(\left(\frac{u \cdot \cos(\alpha) + v \cdot \sin(\alpha)}{\sigma_u} \right)^2 + \left(\frac{-u \cdot \sin(\alpha) + v \cdot \cos(\alpha)}{\sigma_v} \right)^2 \right) \right] \quad (17)$$

2. Lorentz function

$$L = \frac{8 \cdot \pi^3 \cdot \alpha^3}{(4 \cdot \pi^2 \cdot \alpha^2 + r^2)^{\frac{3}{2}}} \quad (18)$$

3. Hat function

$$H = \frac{\sin(\sqrt{u^2 + v^2})}{\sqrt{u^2 + v^2}} \quad (19)$$

Consider the procedure of beam estimation using Gauss function. Thus, beam parameters $\sigma_u(\text{beam})$, $\sigma_v(\text{beam})$, $\alpha(\text{beam})$ correspond to FWHM of two-dimensional Gaussian.

Next, it is necessary to perform a direct two-dimensional Fourier transform of $V_{approx}(u, v)$. We obtain the matrix $D(u, v)$ dividing the result by the Fourier transform of convolution kernel function that is used in gridding (14). The amplitudes of this matrix will be a dirty map or a dirty image of a source.

8.2. CLEAN map

The resulting dirty image generated following the procedure described in Section 8.1 has a number of significant flaws. This image may have negative amplitudes, which does not have any physical meaning. Also there are various noise components. In order to get rid of them, the image needs to be “cleaned”. There are many different methods for “cleaning” a dirty image. This paper will examine the CLEAN algorithm that is used in Imager (see Fig. 6).

The CLEAN algorithm is based on sequentially subtracting of components from a dirty image till a certain threshold is reached. If the matrix $D(u, v)$ is not completely homogeneous, which practically never happens in reality, it will have some maximum. Accordingly, if a certain component is subtracted from a given maximum, a new maximum appears in the image in the same or other coordinates.

The sequence of steps to obtain the resulting or “clean” image of the source using the CLEAN algorithm can be described as follows:

1. Take the matrix of complex numbers $D(u, v)$
2. Obtain the matrix of amplitudes $A(u, v)$ from $D(u, v)$.
3. Declare zero matrix of components $C(u, v)$ with the size of $D(u, v)$.
4. Find the maximum in $A(u, v)$ with (u_{max}, v_{max}) coordinates.
5. For the coordinates of this maximum add unity to the element of $C(u_{max}, v_{max})$ matrix.
6. Subtract beam multiplied by gain from the dirty image $A(u, v)$ (by default gain is 0.1).
7. Return to the search for maximum from the point 4.
8. Repeat points 4–7 as many times as needed.

The obtained matrix $C(u, v)$ is called the CLEAN component map of the reconstructed image. To get a CLEAN image, it is necessary to calculate the sum of the convolution kernel functions applied for each CLEAN component. To do this, the following steps are taken:

1. New matrix $M(u, v)$ is created with the same size as $A(u, v)$ and $C(u, v)$.
2. For each non-zero CLEAN component from $C(u, v)$ a kernel function is calculated (in our case it is Gaussian) with the following parameters: ($A = C_{u,v} \cdot \text{Gain}$, $\sigma_x = \sigma_x(\text{beam})$, $\sigma_y = \sigma_y(\text{beam})$, $\alpha = \alpha(\text{beam})$). Note that Imager can perform CLEAN using different convolution kernel functions.
3. Amplitudes are calculated for each element of $M(u, v)$:

$$M_{u,v} = \sum_{u'=1}^N \sum_{v'=1}^N \psi(C_{u',v'}, u', v', u, v, \sigma_u(\text{beam}), \sigma_v(\text{beam}), \alpha(\text{beam})) \quad (20)$$

In the case of using another kernel function, the set of parameters of the function $\psi(x_1, x_2 \dots x_n)$ under the sum in (20) may change, but the general principle remains the same – for each point the sum of kernel functions for CLEAN components is calculated with given dirty beam parameters (except for the case of using different kernel). The resulting matrix $M(u, v)$ is a pure image or CLEAN image of observed source.

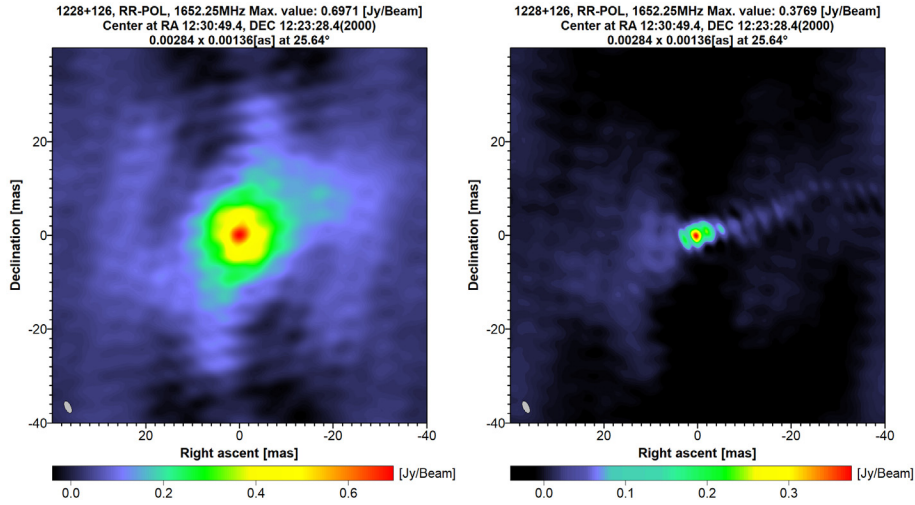


Fig. 6. Example of dirty map (left) and CLEAN map (right) obtained in Imager. The data are from Radioastron mission imaging observations of M87 (1228+126) at L-band (18 cm or 1668 MHz), date/time of observation 04.06.2014 09:00:00–05.06.2014 01:30:00.

9. Self-calibration

In case of self-calibration, the situation is the same as for regular calibration, but instead of real calibration source data a source model or previous CLEAN iteration are used:

$$V_{jk}^{mod}(t) = \sum \sum (I_n \exp\{-2\pi i(u_{jk}x_n + v_{jk}y_n)\} + I_n \exp\{2\pi i(u_{jk}x_n + v_{jk}y_n)\}), \quad (21)$$

where $V_{jk}^{mod}(t)$ is the visibility obtained from the previous iteration of the CLEAN procedure or the proposed model for jk baseline of j and k antennas.

Let us introduce:

$$\frac{V_{jk}^{true}(t)}{V_{jk}^{mod}(t)} = 1, \quad (22)$$

where $V_{jk}^{true}(t)$ is a “true visibility” of a source for jk baseline of j and k antennas, and find a solution for the gain coefficients as

$$\langle V'_{jk}(t) \rangle_{\Delta t} = \langle g_j(t) \rangle_{\Delta t} \langle g_k(t) \rangle_{\Delta t} V_{jk}^{mod}(t), \quad (23)$$

where $V'_{jk}(t)$ is the data that has not been calibrated either in amplitude or in phase, and g_j and g_k are complex gain coefficients for antennas j and k , respectively.

The self-calibration process starts with a large solution interval (from tens of minutes to hours, depending on what calibration is required). Then, with each new iteration of self-calibration it is possible to lower this interval in order to achieve better calibration.

ASL has a capability to analyze $V_{jk}^{true}(t)/V_{jk}^{mod}(t)$ plots with solutions for gain coefficients, which allow to check how the self-calibration proceeds.

For N radio telescopes the relation between the measured visibility $V_{ij}(t_k)$ and “true visibility” $V_{ij}^{true}(t_k)$ obtained at the time moment t_k at baseline (i, j) , $i = 1, 2, \dots, N$, $j = i + 1, i + 2, \dots, N$ can be represented as:

$$V_{ij}(t_k, \nu_l) = g_{ikl} \overline{g_{jkl}} V_{ij}^{true}(t_k, \nu_l) + \varepsilon_{ij}(t_k, \nu_l) \quad (24)$$

From a physical point of view, to estimate $V_{ijkl}^{true}(t)$, it is necessary to synthesize a model of the visibility function $\hat{V}_{ijkl}(t)$, which would minimize a quadratic metric of the following form:

$$\rho = \sum_{\substack{0 < k < K \\ 0 < l < L}} \sum_{\substack{i, j \\ i \neq j}} w_{ij}(t_k \nu_l) \left| V_{ij}(t_k, \nu_l) - g_{ikl} \overline{g_{jkl}} \hat{V}_{ij}(t_k, \nu_l) \right|^2 \xrightarrow{g_i} \min \quad (25)$$

There are three main self-calibration parameters:

1. Time interval to average data for correction functions before the solution.
2. Type of approximation (different variations, robust for layers, etc.).
3. Self-calibration of amplitude, phase or both amplitude and phase at the same time.

Fig. 7 shows a general outline of self-calibration algorithm that was implemented in Astro Space Locator. If the amplitude and phase are not selected, the Clark CLEAN algorithm will be executed (Clark, 1980).

We would like to note that the approach considered above is a generalized self-calibration (GSC), because a joint solution is obtained for amplitudes and phases of gain coefficients and its derivatives. In contrast, other algorithms solve the problem separately, and therefore the developed GSC algorithm is more optimal as it has a global minimum.

10. Multi-frequency imaging

Astro Space Locator is capable of performing multi-frequency imaging (MFI), multi-frequency synthesis (MFS) (see Conway et al., 1990) and multi-frequency analysis of VLBI data. Such approach allows to obtain high quality images interpolated on a given reference frequency as well as to perform an estimate of spectral indices. This approach is very important not only for Space-VLBI missions like Radioastron and Millimetron, but also for ground-based VLBI (Kardashev et al., 2013, 2014, 2017).

Astro Space Locator is capable of performing multi-frequency imaging (MFI), multi-frequency synthesis (see Conway et al., 1990) and multi-frequency analysis of VLBI data. Such approach allows to obtain both high quality images interpolated on a given reference frequency inside of a given bandwidth, as well as reliable estimates of spectral indices for radio sources with power spectrum. This approach is very important not only for Space-VLBI missions like Radioastron and Millimetron, but also for ground-based VLBI arrays like the VLBA, GMVA, EHT. An approach of multi-frequency imaging makes it is possible not only to improve the quality and fidelity of the images and also essentially to derive the morphology of the observed radio sources.

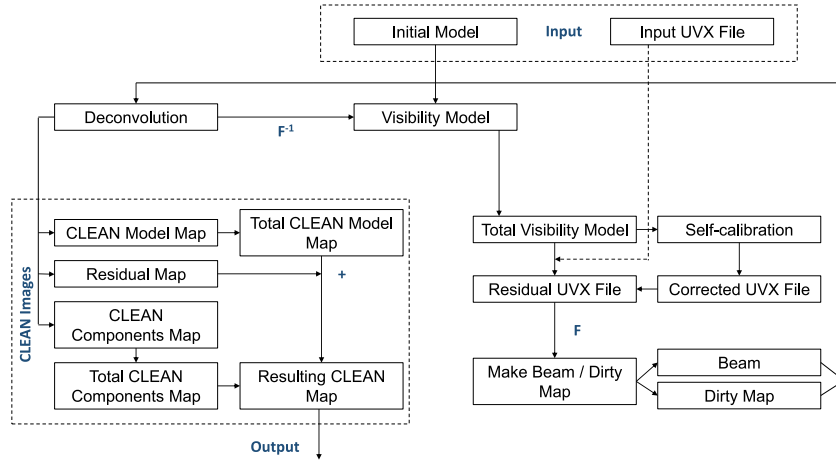


Fig. 7. Diagram of self-calibration procedure implemented in the Astro Space Locator. F and F^{-1} correspond to direct and reverse Fourier transform, respectively.

Let us consider a linear model for intensity $I_{kpq} = I(x_p, y_q, \nu_k)$ of the radio source in a point (x_p, y_q) on the observational frequency ν_k :

$$I_{kpq} = (I_0) + (I_1)_{pq}\beta_k + \dots + (I_{N-1})_{pq} \cdot (\beta_k)^{N-1},$$

$$\beta_k = \frac{\nu_k}{\nu_0} - 1, k = 1, 2, 3, \dots, K, \quad (26)$$

where ν_0 is reference frequency corresponding to the intensity $(I_0)_{pq}$. If the intensity I_{kpq} in the point (x_p, y_q) can be approximated by power law as

$$I_{kpq} = (I_0)_{pq} \cdot \left(\frac{\nu_k}{\nu_0}\right)^{\alpha_{pq}}, \quad (27)$$

then we can present it as

$$I_{kpq} = (I_0)_{pq} e^{\xi_k \alpha_{pq}} \approx (I_0)_{pq} \cdot (1 + \xi_k \alpha_{pq}) \quad (28)$$

where $\xi_k = \ln(1 + \beta_k) \approx \beta_k$, and thus the spectral indices $\alpha_{pq} = \alpha(x_p, y_q)$ can be obtained as

$$(I_1)_{pq} = \alpha_{pq} \cdot (I_0)_{pq} \quad (29)$$

Let us consider a target function

$$\rho = \sum_{k=1}^K \sum_{n=0}^{M-1} \sum_{m=0}^{M-1} w_{knm} \cdot |V_{knm} - \hat{V}_{knm}|^2 \quad (30)$$

where, $w_{knm} = w(u_n, v_m, \nu_k) \geq 0$ are weights, V_{knm} , \hat{V}_{knm} is a measured and a model visibility function respectively,

$$\hat{V}_{knm} = A_k \cdot \sum_{p,q=0}^{M-1} \left[\sum_{l=0}^{N-1} (\hat{I})_{pq} \cdot \beta_k^l \right] \cdot \exp\{-2\pi i \cdot (u_n x_p + v_m y_q)\}, \quad (31)$$

where A_k is a gain coefficient for k^{th} antenna,

$$(\hat{I})_{pq} = \Delta^2 \phi_{pq} \cdot (I_1)_{pq} (1 - x_p^2 - y_q^2)^{-0.5} \quad (32)$$

ϕ_{pq} is a normalized beam, Δ is a grid step. The problem of the optimization can be presented as a solution of the following system of linear equations:

$$(D_0)_{pq} = 0, \dots, (D_{N-1})_{pq} = 0 \quad (33)$$

for a vector of intensity $(\hat{\mathbf{I}})_{rt} = ((\hat{I}_0)_{rt}, (\hat{I}_1)_{rt}, \dots, (\hat{I}_{N-1})_{rt})^T$ where the m^{th} residual map $(D_m)_{pq}$ can be defined as:

$$(D_m)_{pq} = \sum_{k=1}^K \beta_m^k \times \left\{ D_{kpq} - \sum_{i=0}^{M-1} \sum_{l=0}^{M-1} B_{k,p-i,q-l} \cdot \sum_{n=0}^{N-1} (\hat{I}_n)_{il} \cdot \beta_n^k \right\}, \quad (34)$$

where $m = 0, 1, \dots, N-1$ and

$$D_{kpq} = \sum_{n,m=0}^{M-1} w_{knm} \cdot V_{knm} \cdot \exp\{2\pi i (u_n x_p + v_m y_q)\} \quad (35)$$

is a k^{th} “dirty” map at the point (x_p, y_q) ,

$$B_{k,p-i,q-l} = \sum_{n,m=0}^{M-1} w_{knm} \times \exp\{2\pi i [u_n (x_p - x_i) + v_m (y_q - y_l)]\} \quad (36)$$

is a k^{th} “dirty” beam at the point $(x_p - x_i, y_q - y_l)$.

The solution of the problem can be presented as an iterative procedure for a vector $(\hat{\mathbf{I}})_{pq}$:

$$(\hat{\mathbf{I}})_{pq}^{(s)} = (\hat{\mathbf{I}})_{pq}^{(s-1)} + \gamma \mathbf{E}^{-1} \cdot (\mathbf{D})_{pq}^{(s-1)}, \quad (37)$$

and the residual maps $(\mathbf{D})_{rt} = \{(D_0)_{rt}, (D_1)_{rt}, \dots, (D_{N-1})_{rt}\}^T$:

$$(\mathbf{D})_{rt}^s = (\mathbf{D})_{rt}^{s-1} - \hat{\mathbf{B}}_{r-p,t-q} \cdot [(\hat{\mathbf{I}})_{pq}^{(s)} - (\hat{\mathbf{I}})_{pq}^{(s-1)}]. \quad (38)$$

Here $\mathbf{E} = (E_{ij})$ is a positive defined matrix of maximum values of weighted “dirty” beams, $E_{ij} = (\hat{B}_{i+j})_{0,0}$, $i, j = 0, \dots, N-1$, γ is a loop gain. The process of the iteration can be completed if $\varepsilon^{(s-1)} < \varepsilon$, where ε is a given accuracy. Otherwise it is necessary to suppose $s = s + 1$ and to calculate the next $\varepsilon^{(s)}$. Conditions of the convergence of the algorithm above is $0 < \gamma < 2$, $1 \leq N \leq K$.

Implemented algorithm is a multi-frequency linear deconvolution (Likhachev, 2003). It is important to note that it allows to synthesize and analyze VLBI images using the data of different frequencies together and does not require obtaining images at different frequencies separately. MFS comprises the spectral interpolation of the image and can reconstruct the map of spectral indices at a given frequency. Fig. 8 demonstrates an example of multi-frequency synthesis of six frequencies (central image).

11. Pulsar data analysis and reduction

ASL has the following capabilities for analyzing the pulsar VLBI data:

1. Average profile of the pulsar. The average profile can be calculated for single baseline or as a sum of average profiles for all baselines. This utility uses the data correlated by ASC Correlator with incoherent dedispersion (Likhachev et al., 2017). In ASC Correlator incoherent dedispersion uses TEMPO2 pulsar ephemeris (Hobbs et al., 2006).

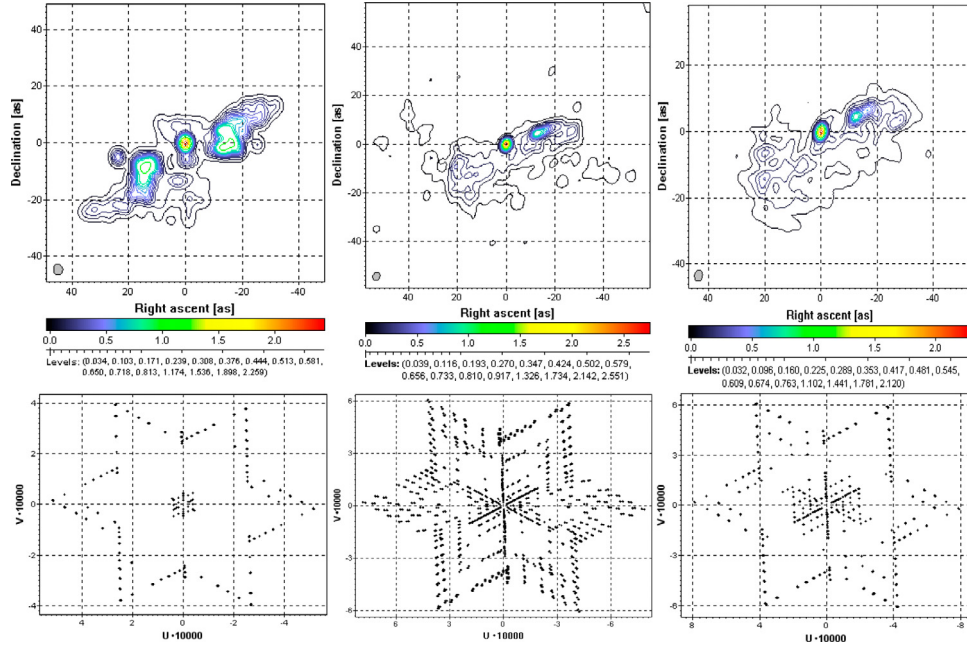


Fig. 8. Example of multi-frequency synthesis using ASL processing algorithms for M87 observations with VLA. Images from left to right: lowest frequency (left), resulting synthesis (center), highest frequency (right). Total six frequencies merged 14.6, 15.1, 21.5, 21.9, 22.9, 23.3 GHz, central frequency for synthesis 19 GHz. Top panel – CLEAN images, bottom panel – corresponding (u, v) coverage.

2. Bandpass calibration of pulsar data.

The main difference between pulsar bandpass and bandpass calibration described in Section 5.2 is that pulsar bandpass uses on-pulse and off-pulse data. For bright sources or high-sensitivity baselines bandpass calibration is performed as follows:

$$C_{bp_i} = \frac{C_{on_i} - C_{off_i}}{\langle C_{off_i} \rangle}, \quad (39)$$

where index i corresponds to the number of spectral channel, C_{bp_i} is an amplitude of the on-pulse spectrum after calibration, C_{on_i} is an amplitude of the on-pulse spectrum, C_{off_i} is an amplitude of the off-pulse spectrum, $\langle C_{off_i} \rangle$ – amplitude of the off-pulse spectrum. All spectra are averaged over the entire observation session. Such bandpass calibration provides additional attenuation of RFI. For low-sensitivity baselines bandpass calibration is performed in a different way:

$$C_{bp_i} = \frac{C_{on_i} - \langle C_{off_i} \rangle}{\langle C_{off_i} \rangle} \quad (40)$$

3. Removal of narrow band RFI. Procedure removes and interpolates the data in spectral channels that have RFI.
4. Dropping weak pulses. This is an automatic filter that removes pulses with intensity lower than the determined threshold.
5. Plotting dynamic (“Delay-Time” diagram) and secondary spectrum (“Delay-Fringe Rate” diagram) of a pulsar. (see Section 3.2). The example of such plots is presented in Fig. 9.

12. Maser data analysis and reduction

ASL software package includes Lineviewer program that can perform data processing and analysis of VLBI data from maser sources (Shchurov et al., 2019).

This program allows to plot the dynamic spectrum and fringe rate–frequency diagrams (see Section 3.2), perform search for

maser details and obtain average spectra. It has an ability to measure the velocity of maser details relative to the local standard of rest (V_{LSR}) or the Earth’s barycenter. This feature is implemented using SOFA library (Wallace, 1996). In addition, Lineviewer provides the ability to perform bandpass using both data from a calibration source and polynomial approximation of a given order.

This program simplifies the search for maser details in auto- and cross-spectra, allows to perform the analysis of velocities of these details and calculate modeled spectra for the sources. Fig. 10 shows the interface of Lineviewer with an example of graphical representation of maser VLBI data.

The spectrum can be averaged both scalar and vector. It is possible to display both the frequency values and the velocity values of the spectral details. At the same time, there is a capability to plot and analyze the phase for average spectra. It allows to identify the various maser details and visually fix the correlation of them.

After bandpass calibration, the selected spectral details can be approximated by M -number of Gaussian functions:

$$S(\nu) = \sum_{i=1}^{M \leq N} A_i \cdot \exp\left(-\frac{(\nu - \nu_i^0)^2}{\sigma_i^2}\right) \quad (41)$$

where $S(\nu)$ – intensity of spectra, ν – frequency, ν_i^0 – central frequency of i th Gaussian, σ_i – Gaussian half-width at half magnitude (HWHM), N – maximum number of Gaussian functions (set by user), M – optimal number of Gaussian functions (determined automatically by the algorithm), $M \leq N$. More details on calculation of M value and detailed description of Lineviewer see Shchurov et al. (2019).

This procedure allows to identify correlating spectral details of the masers, and easily evaluate such parameters of cross-correlated spectral details of the maser as V_{LSR} , detail width and integral intensity.

13. Simulations of synthetic VLBI observations

This section is dedicated to Modeler – a program that allows to simulate VLBI observations.

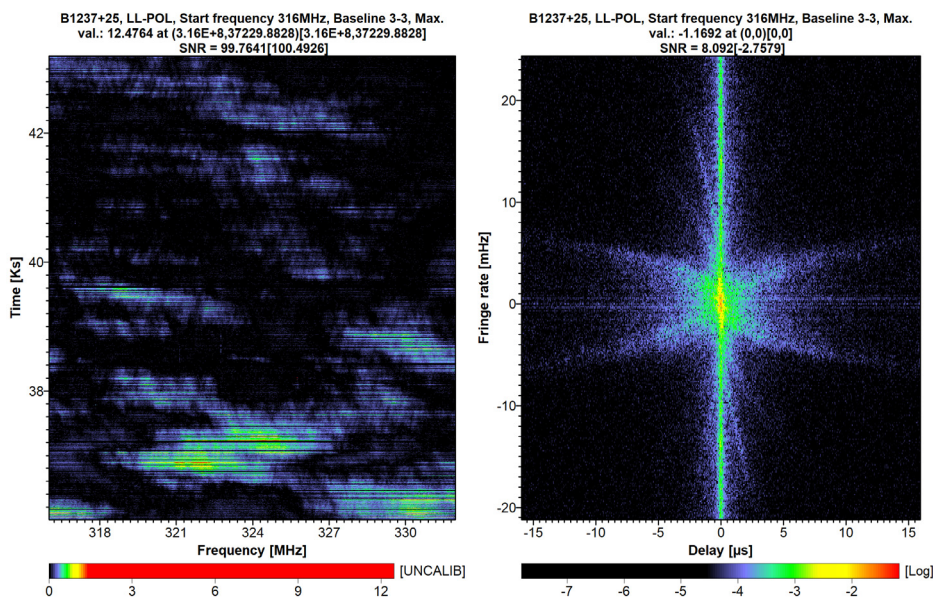


Fig. 9. Example of visualizing the dynamic (frequency–time diagram, left) and secondary (delay–fringe rate diagram, right) spectrum of pulsar in VisView. The amplitude in the secondary spectrum has log scale. Data taken from Radioastron observations of PSR B1237+25 at 327 MHz. Bright spots in the dynamic spectra indicate pulsar scintillation, arcs in the secondary spectra indicate the presence of scattering screens on the line of sight to the pulsar. Arc curvature is connected with the distance to the scattering screen.

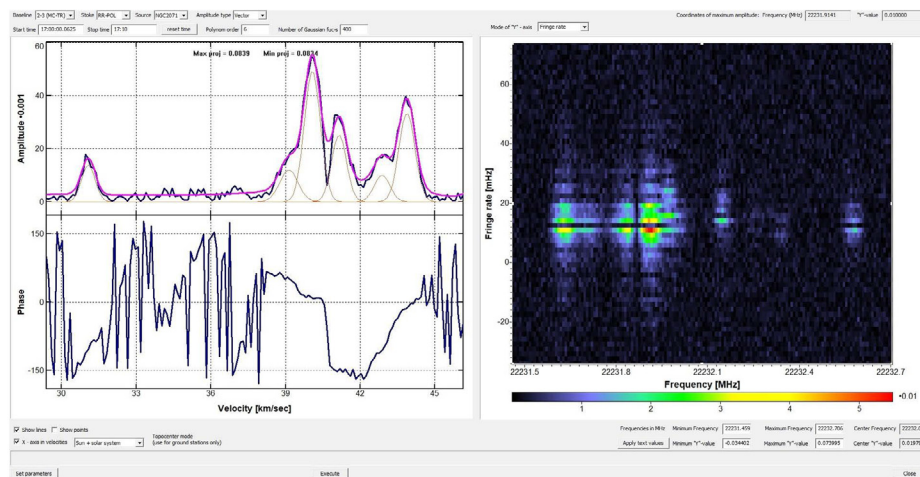


Fig. 10. Interface of Lineviewer program. Left side shows a selected cross-section (amplitude on top and phase on the bottom) of a frequency–fringe rate diagram shown on the right side. A cross-section can be approximated by a set of Gaussian functions (pink line). (For interpretation of the references to color in this figure legend, the reader is referred to the web version of this article.)

It implements a set of mathematical algorithms that can completely simulate any type of VLBI observation: ground, space-ground and, even, space–space. In particular, these are the simulations of interferometer geometry, simulations of a radio source structure and simulations of noise errors. The latter includes simulation of sensitivities.

13.1. Modeling of VLBI geometry

There are two possibilities of setting data for VLBI observation modeling: direct setup in GUI or external setup file. It is possible to insert new source or ground telescope as well as new space antenna if necessary. One can input manually time setup (set of observational segments), start time and duration; frequency setup (set of frequency bands, their number, number of spectral channels and IF bandwidth for each frequency), polarization type of simulated data. ASL Modeler is able to synthesize the VLBI data for any set of polarization parameters (either in terms of

polarization states: circular – various combinations of RCP and LCP; linear – XX, XY, YY, YX; or in terms of Stokes parameters – I, Q, U, V).

With all these parameters assigned Modeler calculates the (u, v) coverage and store it in output UVX file. Note that at this stage there is no information about the intensity distribution. It can be added in “Source modeling” section of Modeler.

13.2. Source modeling

There are two options of intensity distribution assignment: manual setup and external map file.

The first option is a source model/structure editor. The following types of source components are available: delta function, two-dimensional Gaussian, disk, thin ring, thin sphere, rectangle and thick ring. Each component has a number of customizable parameters: flux density F (Jy), major axis (as), minor to major axes ratio, minor axis (as), inclination of the source (deg), distance

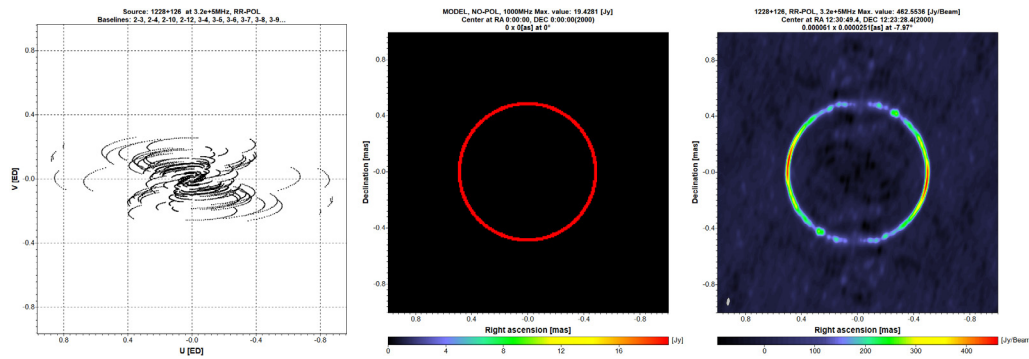


Fig. 11. Example of VLBI data simulations: VLBI geometry or (u, v) coverage (left), source structure (center) and resulting CLEAN image obtained for simulated (u, v) by applying the simulated source structure (right).

from the center of map (as). The configured intensity distribution map can be applied to any real or simulated (u, v) coverage. Additionally, it is possible to compare the real visibility data with the simulated one. Fig. 11 demonstrates simulations of VLBI geometry, source structure and the resulting CLEAN image.

External map file allows using an external source image as an initial source model in the simulations. For example, these can be images obtained from other observations.

13.3. Modeling of noise errors

This part describes the simulation of noise errors of VLBI data. For each baseline it is possible to apply: amplitude and phase errors, reference phase, fringe rate, delay, acceleration of fringe.

Each single telescope has finite sensitivity and it is impossible to observe faint sources. Sensitivity of telescope is represented as System Equivalent Flux Density (*SEFD*, see Section 5.1). Same as single telescope, each baseline is also characterized by its sensitivity, which definition is similar to that of *SEFD*. It can be derived from *SEFD* of both telescopes of given baseline:

$$S = \frac{1}{\sqrt{2\Delta\nu\tau_c}} \sqrt{SEFD_1 \cdot SEFD_2}, \quad (42)$$

where $\Delta\nu$ – bandwidth, τ_c – coherence time. These values can be assigned by user.

Using sensitivities of baselines it is possible to account for distortions in visibility function made by antennae noise. Simulation of such distortions can be generally described in the following way: non-distorted visibility function is added by a complex value with random argument and module that depends on sensitivity of baseline.

14. Utilities

14.1. Calibration data editor

Astro Space Locator has a tool (CalEdit) for editing and viewing amplitude calibration data in the ANTAB format. This program is designed to prepare and analyze calibration files before the procedure of amplitude calibration (see Section 5).

CalEdit allows to plot antenna temperatures over time for all polarizations in the selected observation for each antenna, perform flagging of data points, change their values manually or in automatic mode. The program allows to interpolate measurements with a 5th degree polynomial. Fig. 12 shows an example of visual editing of calibration data.

14.2. Analysis of correlation parameters

There are additional applications AFRDMANY and AFRDAUTO that allow to estimate the coherence of correlated signal for given radio source, baseline, frequency band, start time T_{str} , time step Δt and interval duration ΔT_{max} .

AFRDMANY calculates two characteristic dependencies: visibility amplitude vs. time with a given coherent interval and the behavior of signal-to-noise ratio in time. Thus, it is possible to analyze the behavior of coherence conditions during the observations on a specific baseline.

In AFRDAUTO, in addition to the input parameters of AFRDMANY, the end of the time interval parameter T_{stp} should be specified. This program calculates the values of four time-dependent functions: fringe rate–frequency, delay, signal-to-noise ratio, baseline projection in Earth diameters.

14.3. Supplementary tools

Astro Space Locator includes a number of supplementary tools. AUVXUnion merges (u, v) data of several UVX files into one. Alnterp performs time interpolation of the visibility in UVX file. AGainView is a visualization tool for gains. UVXView and AIDI-View provide text browsing of UVX and IDIFITS data tables. AIMG-toEXM converts any graphical image format (i.e. PNG, BMP, JPEG, etc.) to external map file (EXM), while FTS-EXM converts FITS image format to EXM. Additionally, there is EXM/AMAP viewer. Finally, ASL has an editor of palettes that are used in its programs.

15. Conclusions

In this article we gave an overview of basic functions and principles implemented in the Astro Space Locator software package. ASL is a customizable tool that is easy to use in almost any task associated with VLBI data processing and analysis. At the moment, ASL Locator allows to process correlated VLBI observations, both of the Radioastron mission and VLBI networks such as VLA, VLBA, HSA, EVN.

Astro Space Locator comprises convenient VLBI data visualization and editing. It has all basic calibration tools, including fringe fitting with the 2nd term and powerful self-calibration application.

The CLEAN method of image deconvolution implemented in ASL is comparable to similar software in terms of efficiency (Zuga et al., 2017). The verification data showed a similar accuracy of calculations during the VLBI observations processing. Moreover, the package has a separate application for multi-frequency imaging and analysis.

Astro Space Locator has a great potential in simulating VLBI observations, since it provides the ability to obtain preliminary

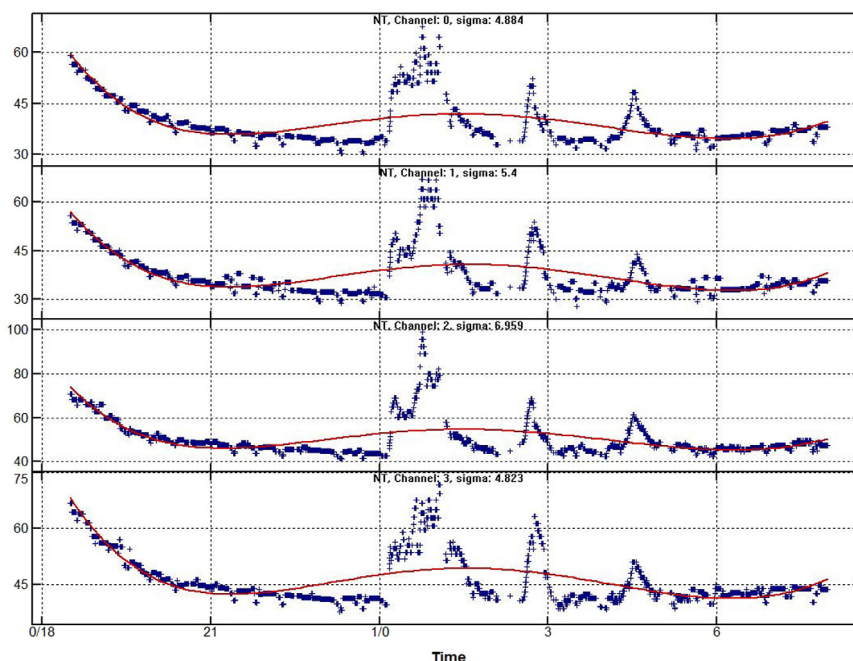


Fig. 12. Example of graphical editing of calibration data in CalEdit. Blue dots correspond to the measures system temperatures for Noto telescope (NT). Four panels demonstrate the system temperature measured in different channels (lower/upper side bands and left/right circular polarizations). Red line shows the polynomial approximation of the system temperature. Any data point can be selected interactively on plot, removed or its value can be changed.

results for a given interferometer configuration and radio source. The output of such modeling can help to improve the results of a future experiment.

The software package has a convenient graphical user interface, number of features and supplementary tools that greatly simplify operations with the correlated VLBI data. It continues to improve as part of the current tasks of ASC LPI and will be used in the Millimetron mission. At the moment, work is under way on the introduction of new image recovery algorithms, developing a full cross-platform support for different operation systems. The latest version package is available on the ftp-server: ftp://www.asc.rssi.ru/ASL_10/ASL10_x64_19-06-20.zip, other versions are available in the corresponding ftp folder: ftp://www.asc.rssi.ru/ASL_10/.

CRediT authorship contribution statement

S.F. Likhachev: Supervision, Conceptualization, Software, Validation. **I.A. Girin:** Software, Validation. **V. Yu. Avdeev:** Writing - original draft, Validation. **A.S. Andrianov:** Writing - original draft, Software, Validation. **M.N. Andrianov:** Software, Validation. **V.I. Kostenko:** Validation, Writing - original draft. **V.A. Ladygin:** Software, Validation. **A.O. Lyakhovets:** Software, Validation, Writing - original draft. **I.D. Litovchenko:** Writing - original draft, Validation. **A.G. Rudnitskiy:** Software, Validation, Writing - original draft, Writing - review & editing, Visualization. **M.A. Shchurov:** Software, Validation, Writing - original draft. **N.D. Utkin:** Writing - original draft, Validation. **V.A. Zuga:** Writing - original draft, Validation.

Declaration of competing interest

The authors declare that they have no known competing financial interests or personal relationships that could have appeared to influence the work reported in this paper.

Acknowledgments

The authors would like to thank both Robert M. Hjellming and Leonid Kogan from NRAO for valuable comments and corrections that were provided during the development of Astro Space Locator software. The authors also would like to thank Taehyun Jung and KVN team for providing the test data for FPT.

References

- Bates, R., McDonnell, M., 1986. *Image Restoration and Reconstruction. In: Application of Linear Systems to Imaging*, Oxford University Press.
- Booch, G., 1993. *Object Solutions: Managing the Object-Oriented Project*. Pearson Education, ISBN:0-8053-0594-7.
- Clark, B.G., 1980. An efficient implementation of the algorithm 'CLEAN'. *Astron. Astrophys.* 89 (3), 377.
- Conway, J.E., Cornwell, T.J., Wilkinson, P.N., 1990. Multi-frequency synthesis: a new technique in radio interferometric imaging. *Mon. Not. R. Astron. Soc.* 246, 490.
- Guirin, I.A., Likhachev, S.F., Chuprikov, A.A., 2006. VLBI Data editing. In: Gabriel, C., Arviset, C., Ponz, D., Enrique, S. (Eds.), *Astronomical Data Analysis Software and Systems XV, Proceedings of the Conference Held 2-5 October 2005 in San Lorenzo de El Escorial, Spain*. In: *Astronomical Society of the Pacific Conference Series*, vol. 351, Astronomical Society of the Pacific, San Francisco, p. 686.
- Hobbs, G.B., Edwards, R.T., Manchester, R.N., 2006. TEMPO2, a new pulsar-timing package - I. An overview. *Mon. Not. R. Astron. Soc.* 369 (2), 655-672. doi:10.1111/j.1365-2966.2006.10302.x, arXiv:astro-ph/0603381.
- Jaeger, S., 2008. The common astronomy software application (CASA). In: Argyle, R.W., Bunclark, P.S., Lewis, J.R. (Eds.), *Astronomical Data Analysis Software and Systems XVII. In: Astronomical Society of the Pacific Conference Series*, vol. 394, p. 623.
- Kardashev, N.S., Alakoz, A.V., Andrianov, A.S., Artyukhov, M.I., Baan, W., Babyshkin, V.E., Bartel, N., Bayandina, O.S., Val'tts, I.E., Voitsik, P.A., Vorobyov, A.Z., Gwinn, C., Gomez, J.L., Giovannini, G., Jauncey, D., Johnson, M., Imai, H., Kovalev, Y.Y., Kurtz, S.E., Lisakov, M.M., Lobanov, A.P., Molodtsov, V.A., Novikov, B.S., Pogodin, A.V., Popov, M.V., Privesenz, A.S., Rudnitski, A.G., Rudnitski, G.M., Savolainen, T., Smirnova, T.V., Sobolev, A.M., Soglasnov, V.A., Sokolovsky, K.V., Filippova, E.N., Khartov, V.V., Churikova, M.E., Shirshakov, A.E., Shishov, V.I., Edwards, P., 2017. RadioAstron science program five years after launch: Main science results. *Solar Syst. Res.* 51 (7), 535-554. doi:10.1134/S0038094617070085.

- Kardashev, N.S., Khartov, V.V., Abramov, V.V., Avdeev, V.Y., Alakoz, A.V., Aleksandrov, Y.A., Ananthakrishnan, S., Andreyanov, V.V., Andrianov, A.S., Antonov, N.M., Artyukhov, M.L., Arkhipov, M.Y., Baan, W., Babakin, N.G., Babushkin, V.E., Bartel, N., Belousov, K.G., Belyaev, A.A., Berulis, J.J., Burke, B.F., Biryukov, A.V., Bubnov, A.E., Burgin, M.S., Busca, G., Bykadorov, A.A., Bychkova, V.S., Vasil'kov, V.I., Wellington, K.J., Vinogradov, I.S., Wietfeldt, R., Voitsik, P.A., Gvamichava, A.S., Girin, I.A., Gurvits, L.I., Dagkesamanskii, R.D., D'Addario, L., Giovannini, G., Jauncey, D.L., Dewdney, P.E., D'yakov, A.A., Zharov, V.E., Zhuravlev, V.I., Zaslavskii, G.S., Zakhvatkin, M.V., Zinov'ev, A.N., Ilinen, Y., Ipatov, A.V., Kanevskii, B.Z., Knorin, I.A., Casse, J.L., Kellermann, K.I., Kovalev, Y.A., Kovalev, Y.Y., Kovalenko, A.V., Kogan, B.L., Komaev, R.V., Konovalenko, A.A., Kopelyanskii, G.D., Korneev, Y.A., Kostenko, V.I., Kotik, A.N., Kreisman, B.B., Kukushkin, A.Y., Kulishenko, V.F., Cooper, D.N., Kut'kin, A.M., Cannon, W.H., Laktionov, M.G., Lisakov, M.M., Litvinenko, L.N., Likhachev, S.F., Likhacheva, L.N., Lobanov, A.P., Logvinenko, S.V., Langston, G., McCracken, K., Medvedev, S.Y., Melekhin, M.V., Menderov, A.V., Murphy, D.W., Misyakina, T.A., Mozgovoi, Y.V., Nikolaev, N.Y., Novikov, B.S., Novikov, I.D., Oreshko, V.V., Pavlenko, Y.K., Pashchenko, I.N., Ponomarev, Y.N., Popov, M.V., Pravin-Kumar, A., Preston, R.A., Pyshnov, V.N., Rakhimov, I.A., Rozhkov, V.M., Romney, J.D., Rocha, P., Rudakov, V.A., Räisänen, A., Sazankov, S.V., Sakharov, B.A., Semenov, S.K., Serebrennikov, V.A., Schilizzi, R.T., Skulachev, D.P., Slysh, V.I., Smirnov, A.I., Smith, J.G., Soglasnov, V.A., Sokolovskii, K.V., Sondaar, L.H., Stepan'yants, V.A., Turygin, M.S., Turygin, S.Y., Tuchin, A.G., Urpo, S., Fedorchuk, S.D., Finkel'shtein, A.M., Fomalont, E.B., Fejes, I., Fomina, A.N., Khapin, Y.B., Tsarevskii, G.S., Zensus, J.A., Chuprikov, A.A., Shatskaya, M.V., Shapirovskaya, N.Y., Sheikhet, A.I., Shirshakov, A.E., Schmidt, A., Shnyreva, L.A., Shpilevskii, V.V., Ekers, R.D., Yakimov, V.E., 2013. "RadioAstron"—A telescope with a size of 300 000 km: Main parameters and first observational results. *Astron. Rep.* 57, 153–194. doi:10.1134/S1063772913030025, arXiv:1303.5013.
- Kardashev, N.S., Novikov, I.D., Lukash, V.N., Pilipenko, S.V., Mikheeva, E.V., Bisikalo, D.V., Wiebe, D.S., Doroshkevich, A.G., Zasov, A.V., Zinchenko, I.I., Ivanov, P.B., Kostenko, V.I., Larchenkova, T.I., Likhachev, S.F., Malov, I.F., Malofeev, V.M., Pozanenko, A.S., Smirnov, A.V., Sobolev, A.M., Cherepashchuk, A.M., Shchekinov, Y.A., 2014. Review of scientific topics for the Millimetron space observatory. *Phys.-Usp.* 57 (12), 1199–1228. doi:10.3367/UFNe.0184.201412c.1319, arXiv:1502.06071.
- Kim, J., Lee, J.-E., Choi, M., Bourke, T.L., II, N.J.E., Francesco, J.D., Cieza, L.A., Dunham, M.M., Kang, M., 2015. Infrared and radio observations of a small group of protostellar objects in the molecular core, L1251-C. *Astrophys. J. Suppl. Ser.* 218 (1), 5. doi:10.1088/0067-0049/218/1/5.
- Kogan, L., 1995. Effect of digitizers errors on the cross and auto correlation response of an FX correlator, VLBA Scientific Memos, 9.
- Likhachev, S., 2003. Generalized self-calibration for space VLBI image reconstruction. In: Payne, H.E., Jedrzejewski, R.L., Hook, R.N. (Eds.), *Astronomical Data Analysis Software and Systems XII*. In: *Astronomical Society of the Pacific Conference Series*, vol. 295, p. 191.
- Likhachev, S.F., Kostenko, V.I., Girin, I.A., Andrianov, A.S., Rudnitskiy, A.G., Zharov, V.E., 2017. Software correlator for radioastron mission. *J. Astron. Instrum.* 6, 1750004–1750131. doi:10.1142/S2251171717500040, arXiv:1706.06320.
- Palmer, J.W., 1996. AIPS – astronomical image processing system. *Starlink User Note* 207.
- Petrov, L., Kovalev, Y.Y., Fomalont, E.B., Gordon, D., 2011. The very long baseline array galactic plane survey – VGaPS. *Astrophys. J.* 142 (2), 35. doi:10.1088/0004-6256/142/2/35, arXiv:1101.1460.
- Rioja, M., Dodson, R., Malarecki, J., Asaki, Y., 2011. Exploration of source frequency phase referencing techniques for astrometry and observations of weak sources with high frequency space very long baseline interferometry. *Astron. J.* 142 (5), 157. doi:10.1088/0004-6256/142/5/157, arXiv:1110.0267.
- Rumbaugh, J., 1991. *Object-Oriented Modeling and Design*. With others. Prentice Hall, ISBN:0-13-629841-9.
- Shchurov, M.A., Avdeev, V.Y., Girin, I.A., Kostenko, V.I., Likhachev, S.F., Lodigin, V.A., Rudnitskiy, A.G., Shaykhutdinov, A.R., 2019. Lineviewer program of the astro space locator (ASL) package for constructing and processing averaged spectra. *Bull. Lebedev Phys. Inst.* 46 (4), 133–137. doi:10.3103/S1068335619040079.
- Shepherd, M.C., 1997. Difmap: an interactive program for synthesis imaging. In: Hunt, G., Payne, H. (Eds.), *Astronomical Data Analysis Software and Systems VI*. In: *Astronomical Society of the Pacific Conference Series*, vol. 125, p. 77.
- Thompson, A.R., Moran, J.M., Swenson, J., 2017. *Interferometry and Synthesis in Radio Astronomy*, third ed. doi:10.1007/978-3-319-44431-4.
- Wallace, P.T., 1996. The IAU SOFA initiative. In: Jacoby, G.H., Barnes, J. (Eds.), *Astronomical Data Analysis Software and Systems V*. In: *Astronomical Society of the Pacific Conference Series*, vol. 101, p. 207.
- Zhao, Z., An, T., Lao, B., 2019. VLBI network simulator: An integrated simulation tool for radio astronomers. *J. Korean Astron. Soc.* 52, 207–216, arXiv:1808.06726.
- Zuga, V.A., Rudnitskiy, A.G., Likhachev, S.F., 2017. Comparative analysis of image reconstruction algorithms of the ASL and CASA software packages. *Bull. Lebedev Phys. Inst.* 44, 21–24. doi:10.3103/S1068335617010067.